Isomeric ratio measurements for the radiative neutron capture ^{176}Lu(n,γ) at the LANL DANCE facility

D. Denis-Petit,[1,*] O. Roig,[1] V. Méot,[1] B. Morillon,[1] P. Romain,[1] M. Jandel,[2] T. Kawano,[2] D. J. Vieira,[2] E. M. Bond,[2] T. A. Bredeweg,[2] A. J. Couture,[2] R. C. Haight,[2] A. L. Keksis,[2] R. S. Rundberg,[2] and J. L. Ullmann[2]

[1]*CEA DAM DIF, F-91297 Arpajon, FRANCE*

[2]*Los Alamos National Laboratory, Los Alamos, New Mexico 87545, USA*

The isomeric ratios for the neutron capture reaction ^{176}Lu(n,γ) to the $J^{\pi} = 5/2^-$, 761.7 keV, $T_{1/2} = 32.8$ ns and the $J^{\pi} = 15/2^+$, 1356.9 keV, $T_{1/2} = 11.1$ ns levels of ^{177}Lu have been measured for the first time. The experiment was carried out with the Detector for Advanced Neutron Capture Experiments (DANCE) at the Los Alamos National Laboratory. Measured isomeric ratios are compared with TALYS calculations using different models for photon strength functions, level densities, and optical potentials. In order to reproduce the experimental γ-ray spectra, a low-energy resonance must be added in the photon strength function used in our Hauser-Feshbach calculations.

I. INTRODUCTION

Neutron capture cross sections are of high interest in nuclear astrophysics to investigate the *s* process in which the synthesis of heavy elements is dominated by neutron-induced reactions. In this context, partial cross sections feeding the ground states or isomers are particularly crucial in certain cases of the *s*-process nucleosynthesis [1–3] or of astrophysical environments such as neutron stars or supernovae where reactions on the isomeric states can occur [4,5]. For instance, due to the presence of a low-lying isomeric state, the *s*-only ^{176}Lu exhibits a thermally enhanced β-decay rate [6], making it a sensitive branch point for estimating neutron density and temperature at the nucleosynthesis site [3].

From the first studies on isomeric states [7,8], the isomeric ratio, defined here as the ratio of isomeric over total (n,γ) cross sections, was always seen as a pertinent parameter to characterize the γ-ray cascade following the decay of the compound nucleus state. Parameters required to estimate the neutron capture cross sections—such as the spin distribution of the compound nucleus, the level density, and the photon strength function—can be determined from the isomeric ratio measurements. In fast neutron capture, few measurements of these isomeric ratios were performed. Recent preliminary studies of capture γ-ray cascades after neutron capture of ^{235}U revealed an unexpectedly large population of isomeric states in the ^{236}U compound nucleus, suggesting deficiencies in existing theoretical models [9]. This result clearly shows that the initial spin distribution of the compound nucleus and the nuclear structure of low-lying levels have a large impact on the isomer feeding [10]. This conclusion was also experimentally stressed by Ledoux *et al.* [11] using an isomeric ratio measurement by neutron activation for the ^{177m}Lu $J^{\pi} = 23/2^-$ isomeric state. In the particular case of ^{176}Lu$(n,\gamma)^{177}$Lu, similar discrepancies in the intensities of primary and secondary γ-ray transitions

were observed by Rekstad, Tveter *et al.* [12,13] and Aldea, Becvar *et al.* [14].

Several methods have been used to measure the isomeric ratio in neutron capture reactions: the activation method when the lifetimes of the capture reaction product are sufficiently long [11,15,16], the calorimetry method measuring the total γ energy when excitation energy of isomeric states is sufficiently high compared to the detector energy resolution [17,18], and the method combining time and calorimetry for short lifetimes and high excitation energy of isomeric states [19,20].

In this paper, we describe a new method using the high-efficiency and granularity of the Detector for Advanced Neutron Capture Experiments (DANCE) array (Los Alamos National Laboratory) driven by a digital data acquisition system. We have measured the isomeric ratios for the two short-lifetime isomers of ^{177}Lu formed by radiative capture reactions on ^{176}Lu, which is one of two natural isotopes with the highest ground-state spin ($J^{\pi} = 7^-$).

The experimental setup used to measure the γ spectra is described in Sec. II. The data analysis and the technique used to identify the isomers are presented in Sec. III. Section IV is devoted to simulations of the γ cascade and of the detector needed to obtain the detection efficiencies. In Sec. V the measured isomeric ratios are presented and compared to calculations performed with the TALYS [21] and CoH$_3$ [22] nuclear reaction codes.

II. EXPERIMENTAL SETUP

A. The LANSCE facility

The LANSCE linear accelerator provides an 800 MeV proton beam. This beam is compressed using the proton storage ring (PSR) to a 250 ns pulse. A 100 μA beam is delivered at a rate of 20 Hz onto the spallation neutron source in the Lujan Center of LANSCE [23], which is a tungsten target. The neutrons produced are moderated in water located just downstream from the neutron production target. The Detector for Advanced Neutron Capture Experiments (DANCE) is located at the end of a 20.25 m long flight path, named FP14.

B. The DANCE array

The DANCE array is composed of 160 barium fluoride (BaF_2) scintillators. This nearly 4π detector is used to measure the total γ-ray energy coming from the neutron capture on the target located at its center. This one is placed in a vacuum beam tube surrounded by a 6 cm thick ^{6}LiH neutron-scattering shield. This ^{6}LiH shell attenuates the scattered neutrons flux by a factor of about 100 for the highest neutron energies [24]. The pulses from the BaF_2 crystals are recorded using two Acqiris DC265 digitizers with a sampling rate of 500 MHz (2 ns per point) and a resolution of 8 bits [25]. Important information such as the fast and slow scintillator light output integrals used for the pulse shape discrimination (PSD) and the time of the pulse are extracted from the digitized waveforms. For the latter, the position of the leading edge is determined using a constant fraction discriminator (CFD) algorithm. Both segmented and continuous modes of the DANCE acquisition [25] were used to accurately determine each part of the neutron time-of-flight spectrum over the wide energy range. The segmented mode includes a γ-γ coincidence in a time window of 200 ns triggered by a γ threshold of about 150 keV. In this case, the acquisition system gathers data with a fixed dead time of 3.5 μs over the 14 ms time-of-flight range thus including thermal neutron energy. The continuous mode consists of two 250 μs wide time-of-flight windows corresponding to the memory buffer of data collected with no dead time. The covered incident neutron energy range depends on the choice of time acquisition delays and widths for both windows. In our case the continuous mode is used for the neutron energy above 8.5 eV and up to 100 keV.

The DANCE array provides the γ-sum energy E_Σ, the multiplicity of crystal hits, and the γ-ray energies and times from each crystal for each γ cascade following the neutron capture. To take into account the Compton effect inside the ball array, a cluster of hits is defined when at least one neighboring crystal is hit. Cluster multiplicity M and cluster γ-ray energies E_γ determined for each γ cascade are also available. A cluster time is also defined as the mean of all the crystal times which compose this cluster.

C. The targets

The ^{176}Lu target is unique, with an isotopic enrichment of nearly 99.995% for the mass of 0.542 ± 0.022 mg/cm^2 and a deposit diameter of 7 mm on a 1 μm aluminized Mylar foil. This high level of enrichment was achieved using a mass spectrometer, SIDONIE, available at the CSNSM laboratory (Orsay, France).

To evaluate the background due to neutron scattering on the target backing, we used a blank target which is composed of the same backing material as the Lu target.

III. DATA ANALYSIS

The isomeric cross-section ratio R_{iso} of an isomer located at an excitation energy E_{iso} is defined as the ratio of the isomer production cross section σ_{iso} and the total (n,γ) cross section

$\sigma_{tot}(n,\gamma)$:

$$R_{iso} = \frac{\sigma_{iso}}{\sigma_{tot}(n,\gamma)} = \frac{N_{iso}}{N_{casc}}, \qquad (1)$$

where N_{iso} is the number of events populating the considered isomer and N_{casc} is the number of produced γ cascades which reflects the number of ^{177}Lu formed by radiative capture reactions. Experimentally, the DANCE detection efficiencies must be taken into account to deduce N_{iso} and N_{casc} from the experimental ones N_{iso}^{exp} and N_{casc}^{exp}. Thus, Eq. (1) can be rewritten as

$$R_{iso} = \frac{N_{iso}}{N_{casc}} = \frac{N_{iso}^{exp}}{N_{casc}^{exp}} \frac{\epsilon_{casc}}{\epsilon_{iso}}, \qquad (2)$$

where N_{iso}^{exp} is the number of isomer deexcitation detected by DANCE, N_{casc}^{exp} is the number of detected γ cascades, ϵ_{casc} is the cascade detection efficiency, and ϵ_{iso} is the isomer detection efficiency.

In this section, we will describe how N_{iso}^{exp} and N_{casc}^{exp} are determined. The simulations used to obtain the ϵ_{casc} and ϵ_{iso} efficiencies are described in Sec. IV. In this section, only the continuous acquisition mode is used which corresponds to neutron energies between 8.5 eV and 100 keV. The segmented mode, for neutron energies below 8.5 eV, cannot be used for the isomer studies because of the fixed dead time of 3.5 μs after each trigger. However, this mode is used to validate our γ-cascade simulations.

A. Selection of the isomers

Our method to determine isomeric cross section ratios consists of a careful study of γ cascades using the time information of each γ ray of the cascade. In a large coincidence window of 250 ns defined in the offline analysis, all γ rays following the neutron capture are recorded and define a capture event. The first γ rays in this window arriving in a 20 ns width window define the prompt γ cascade. The other γ rays are described as delayed γ rays. The duration of the prompt cascade is defined as the time mean of the individual clusters which compose this cascade. With our method, the decays of the $T_{1/2} = 155$ μs and the $T_{1/2} = 160.4$ d isomers cannot be measured. As their direct feedings are expected to be very low, the influence of these isomers on the total number of γ cascades can be neglected. The decay of the $T_{1/2} = 130$ ns isomer also cannot be measured as its decay proceeds by the emission of a γ ray with an energy below the DANCE detection threshold, which is 150 keV.

The selection of events with a particular number of delayed γ rays highlights particular isomer decays. This selection is illustrated in Fig. 1 for cluster multiplicities summed from $M = 3$ to $M = 6$ without any selection in the cascade sum energy. The multiplicity M is the total cluster multiplicity of the cascade, which includes the prompt and delayed γ rays.

In Fig. 1, the following γ-ray spectra are presented: the spectrum with only one delayed γ ray for the Lu and blank targets and the spectrum with two delayed γ rays for the Lu target.

The spectrum which represents the events with only one delayed γ ray ($M - 1$ prompt γ rays) exhibits two peaks
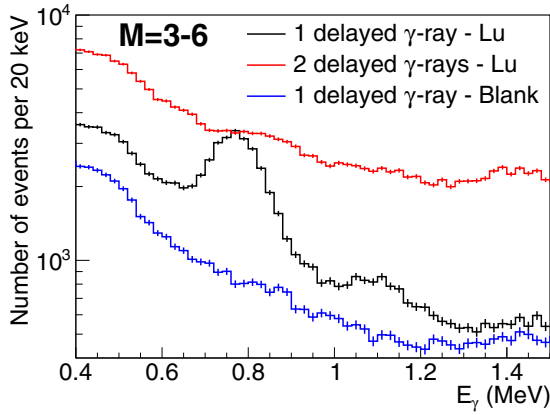
FIG. 1. Delayed γ-ray spectra obtained with the DANCE array for $M = 3$ to $M = 6$ cluster multiplicities. Spectra with only one delayed γ ray for the Lu and the blank targets and two delayed γ rays for the Lu target are plotted.

located at 762 keV and around 1.1 MeV. These peaks are not present in the case of the blank target, which indicates that they are associated with the ^{177}Lu decay. To identify these peaks, energy gates taking into account the BaF$_2$ energy resolution are defined around the full energy peaks at 762 keV and 1.1 MeV on the spectrum with one delayed γ ray.

In Fig. 2, the energy-gated time spectra which represent the difference between the time of the prompt γ cascade and the delayed γ ray are plotted for the Lu and blank targets for multiplicities summed from $M = 3$ to $M = 6$. As we select capture events with a low number of delayed γ rays, those where the prompt cascade is not in the first 20 ns of the large coincidence window (250 ns) are rejected. Due to the selection of a high multiplicity prompt cascade, the energy-gated time spectra are not contaminated by the low-multiplicity background events which are removed. The isomer exponential decays are clearly visible for the Lu target whereas the time spectra are flat for the blank target except for the lowest time when the influence of the prompt cascade can be observed. An exponential fit, $f(t) = A_0 \exp(-\frac{\ln 2}{T} t) + B$, is performed to extract the lifetimes and the number of detected isomers for this multiplicity range. The fit parameters are reported in Table I. According to the fit results, the peaks located at 762 keV and 1.1 MeV are associated with isomers with lifetimes of $T_{1/2} = 35.0 \pm 0.9$ ns and $T_{1/2} = 10.8 \pm 0.5$ ns, respectively. In the nuclear table from [26], these two isomers are identified as the $J^\pi = 5/2^-$, $T_{1/2} = 32.8 \pm 2.4$ ns level located at 761.7 keV and the $J^\pi = 15/2^+$, $T_{1/2} = 11.1 \pm 1.0$ ns level located at 1356.9 keV, respectively. In this database, the $T_{1/2} = 11.1$ ns isomer is fed by another isomer located at 1437.9 keV whose

TABLE I. Results from the time decay fits performed for the studied isomers.

Isomer	T (ns)	A_0 (counts/ns)	B (counts/ns)
761.7 keV	35.0 (9)	522.8 (115)	43.1 (13)
1356.9 keV	10.8 (5)	750.3 (622)	28.2 (5)
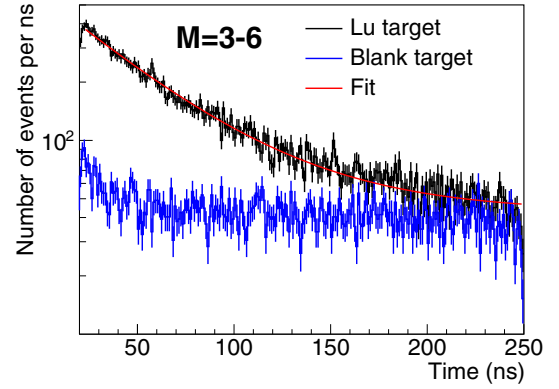
(a) $E_{iso} = 761.7$ keV, $T_{1/2} = 32.8$ ns isomer
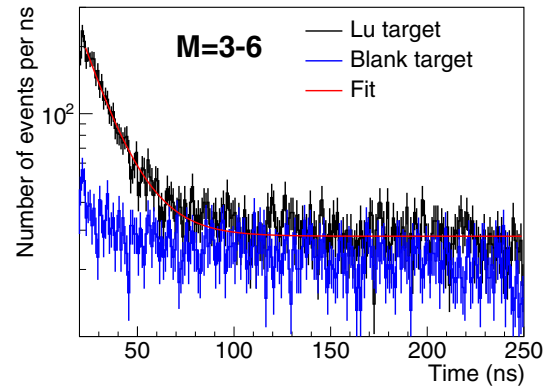
(b) $E_{iso} = 1356.9$ keV, $T_{1/2} = 11.1$ ns isomer

FIG. 2. Time spectra obtained by applying energy gates on energy spectra with one delayed γ ray for the Lu and blank targets. The exponential fits used to obtain the isomer population and lifetime are also plotted.

lifetime is not accurately known: $T_{1/2} < 13$ ns. As we have not succeeded in fitting the decay curve of Fig. 2(b) with two lifetimes, either the lifetime of the 1437.9 keV isomer is about a few ns or it is weakly populated.

The number of isomer deexcitations detected by DANCE $N_{\text{iso}}^{\text{exp}}$ is deduced from these fits by

$$N_{\text{iso}}^{\text{exp}} = \frac{A_0 T}{\ln 2\, I_{1\gamma}}, \tag{3}$$

where $I_{1\gamma}$ is the probability that the isomer decays by only one delayed γ ray, taking into account the DANCE detection threshold and the level scheme which is presented in Fig. 3. The deexcitation of the $T_{1/2} = 32.8$ ns isomer to the ground state mainly proceeds by the emission of only one γ ray at 761.7 keV [γ intensity of $I_\gamma(761.7) = 70.5 \pm 2.8\%$]. The full energy peak located at 762 keV is thus clearly visible in the spectrum with only one delayed γ ray. Thus, we have $I_{1\gamma} = I_\gamma(761.7) = 70.5 \pm 2.8\%$ for the 761.7 keV isomer.

The $T_{1/2} = 11.1$ ns isomer mainly decays by the emission of a γ ray at 1088.1 keV [$I_\gamma(1088.1) = 71.0 \pm 4.4\%$ if the
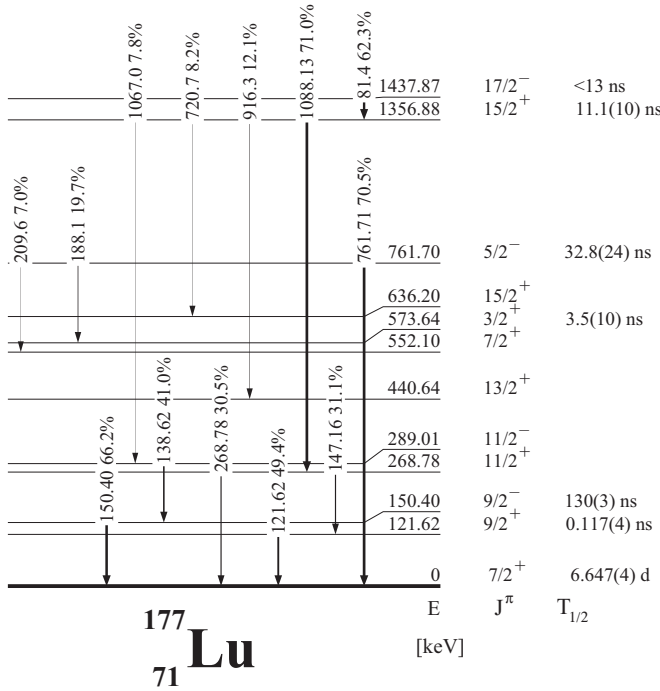
FIG. 3. Partial level scheme of ^{177}Lu [26,27]. The absolute γ intensities are reported.

1206 keV γ-ray intensity is considered to be negligible[1]] to the $J^\pi = 11/2^+$ level located at 268.8 keV. The deexcitation of the latter proceeds by the emission of a γ ray at 147.2 keV to the $J^\pi = 9/2^+$ 121.62 keV level or by the emission of a γ ray at 268.8 keV to the ground state. As the internal conversion coefficients associated with these transitions have not been measured, we have calculated them with the BRICC code [28]: $\alpha_e(147.2) = 1.13\,(4)$ and $\alpha_e(268.8) = 0.1071\,(15)$. The deduced γ intensities are $I_\gamma(147.2) = 31.1 \pm 0.7\%$ and $I_\gamma(268.8) = 30.5 \pm 0.9\%$. As the energy threshold applied on the DANCE crystal energy is 150 keV, the 147.2 keV γ ray cannot be measured. In this case, the majority of the decay of the $T_{1/2} = 11.1$ ns isomer is seen as only one delayed γ-ray emission. Due to the low energy resolution of the BaF$_2$ detectors, the peak at 1088.1 keV is blended with the peak at 1067.0 keV also associated with the decay of the $T_{1/2} = 11.1$ ns. As shown in Fig. 3, the emission of the 1067.0 keV γ ray is followed by the emission of two γ rays which are below the DANCE detection threshold (γ rays at 121.6 and 150.4 keV). By taking into account the DANCE detection threshold, the decay of the $T_{1/2} = 11.1$ ns isomer is mainly detected with only one delayed γ ray. Thus we have $I_{1\gamma} = I_\gamma(1088.1)[1 - I_\gamma(268.8)] + I_\gamma(1067.0) = 56.8 \pm 4.2\%$ for this isomer.

B. Number of detected cascades

The number of detected cascades $N_{\mathrm{casc}}^{\mathrm{exp}}$ is summed for cluster multiplicities ranging from $M = 3$ to $M = 6$ because

---

[1]Its intensity is not accurately known and its placement in the level scheme is uncertain [26].

the background is too high for multiplicities less than 3. It is determined, for each multiplicity, by integrating the total energy E_Σ spectrum on a wide energy range around the neutron separation energy $S_n = 7.073$ MeV: $E_\Sigma \in [3.5, 7.5]$ MeV. The case where there is only one cluster hit in the first 20 ns of the large coincidence window of 250 ns (total cluster multiplicity M) corresponds to a background event and is corrected. In this case, the sum energy is calculated by summing the residual γ-ray energies of the events and is reported in the sum energy spectrum corresponding to the $M - 1$ multiplicity. The background spectrum is obtained in the same way for each multiplicity with the blank target. This background is composed of γ rays emitted following the neutron capture on hydrogen (γ rays at 2.2 MeV) from the ^{6}LiH ball and on barium isotopes (E_Σ around 5 MeV for neutron capture on ^{138}Ba, around 7 MeV for neutron capture on ^{134,136}Ba, and around 8.5–9 MeV for capture on ^{135,137}Ba).

Before the background spectrum subtraction, it is normalized on the Lu spectrum between 8 and 9.5 MeV where only neutron captures on Ba take place for both targets. This subtraction is performed for each multiplicity and for the whole neutron energy range. The total energy spectra (raw, background, and background subtracted) are presented in Fig. 4 for multiplicities ranging from 3 to 6. The areas which represent the integral limits are also plotted.

IV. SIMULATIONS OF THE ^{177}Lu γ DECAY

A. Calculations

The cascade and isomer detection efficiencies are calculated with GEANT4 [29] simulations of the DANCE detector [30] and using theoretical γ cascades calculated with our Monte Carlo code EVITA, which is based on the Hauser-Feshbach formalism. This code is able to reproduce a γ-cascade event using all available information for each nucleus involved in the capture reaction. The level scheme and neutron transmission coefficients used as inputs by EVITA are calculated by the TALYS code [21] (version 1.4) and optimized based on the specific available information on the desired isotope and reaction. The models and parameters used in these simulations are described below. Some parameters are adjusted to reproduce the DANCE data and to get accurate detection efficiencies.

1. Optical potential

The optical potential is used to determine the neutron transmission coefficients in the Hauser-Feshbach formalism. In our calculations, we use a deformed optical potential developed at CEA and specially optimized for the $n + ^{176}$Lu reaction [31].

2. Nuclear level scheme

The nuclear level scheme used in our calculations (EVITA/TALYS) is given in the TALYS package. It is based on the RIPL-3 nuclear data library [32]. In our calculations, 80 discrete levels (excitation energy up to 1480 keV) above the ground state are taken into account to observe the decay of the isomer located at 1356.9 keV. The cumulative discrete level density is plotted in Fig. 5 with the two studied isomers. In
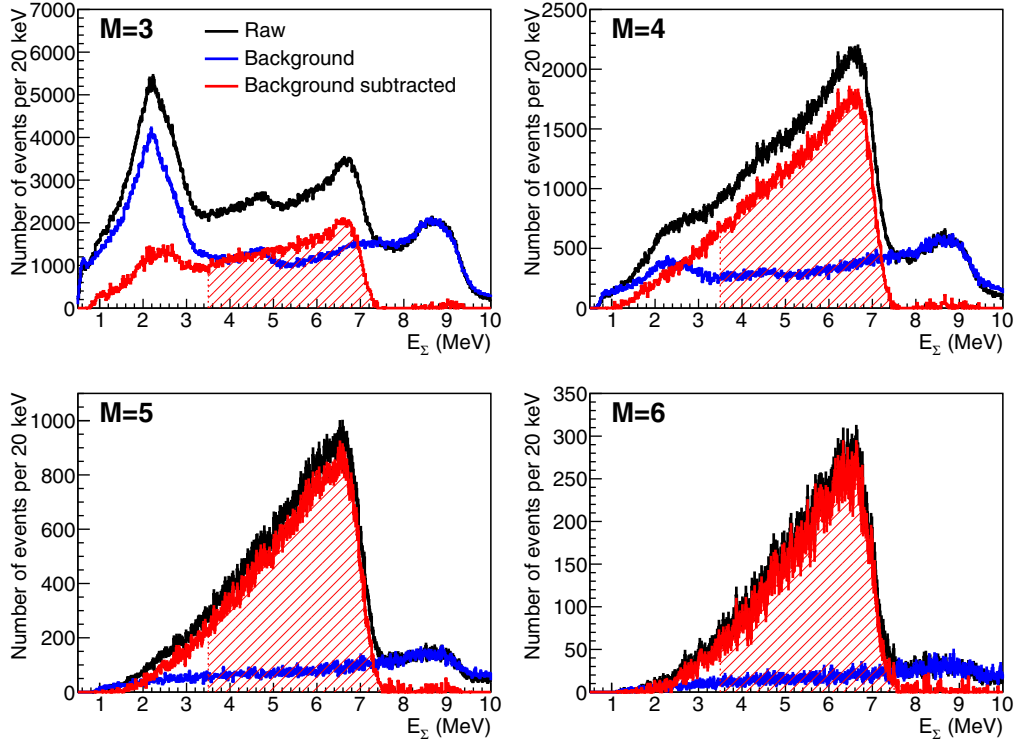
FIG. 4. Total energy spectra for the ^{176}Lu and the blank targets. The background-subtracted spectrum, used to determine the number of detected cascades is also plotted with the integral limits.

the EVITA/TALYS calculations, the decay of the isomers with a lifetime higher than 200 ns is inhibited in order to reproduce experimental conditions.

3. Nuclear level density

The Gilbert and Cameron model [33] is used for the nuclear level density (NLD) in our calculations. In this model, the NLD is divided in two regions: below an excitation energy E_M the constant temperature (CT) model is used and the Fermi gas (FG) model is applied for energies higher than E_M. The NLD

FIG. 5. Cumulative discrete and continuous level density. The positions of the isomers of interest and of the last discrete level taken into account are also plotted.

$\rho(E_x, J, \Pi)$ is thus given by

$$\rho(E_x, J, \Pi) = \begin{cases} \frac{1}{2} R(E_x, J) \rho^{CT}(E_x) & \text{if } E_x \leqslant E_M, \\ \frac{1}{2} R(E_x, J) \rho^{FG}(E_x) & \text{if } E_x \geqslant E_M, \end{cases} \quad (4)$$

where

$$\rho^{CT}(E_x) = \frac{1}{T_0} \exp\left(\frac{E_x - E_0}{T_0}\right) \quad (5)$$

and

$$\rho^{FG}(E_x) = \frac{1}{\sqrt{2\pi}\sigma(E_x)} \frac{\sqrt{\pi}}{12} \frac{\exp(2\sqrt{a(E_x)(E_x - \Delta)})}{a(E_x)^{1/4}(E_x - \Delta)^{5/4}}. \quad (6)$$

In Eq. (6), the level density parameter a and the spin cutoff parameter σ are given by

$$a(E_x) = \widetilde{a}\left(1 + \delta W \frac{1 - \exp(-\gamma[E_x - \Delta])}{E_x - \Delta}\right) \quad (7)$$

and

$$\sigma^2(E_x) = 0.01389 \frac{A^{5/3}}{\widetilde{a}} \sqrt{a(E_x)(E_x - \Delta)}. \quad (8)$$

The spin distribution $R(E_x, J)$ of Eq. (4) is given by

$$R(E_x, J) = \frac{2J + 1}{2\sigma(E_x)^2} \exp\left[-\frac{(J + 1/2)^2}{2\sigma(E_x)^2}\right]. \quad (9)$$

In the case of ^{177}Lu, the different parameters are $E_M = 5.17$ MeV, $E_0 = -0.918$ MeV, $T = 0.536$ MeV, $\widetilde{a} = 19.4$ MeV^{-1}, $\delta W = 1.75$ MeV, $\gamma = 0.077$ MeV^{-1}, $\Delta = 0.902$ MeV.
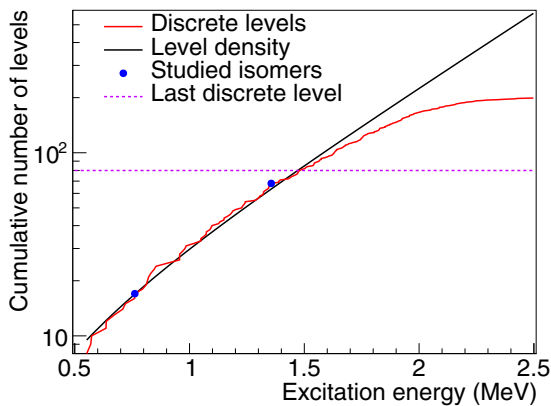
In Fig. 5, the cumulative number of levels as a function of the excitation energy are plotted in the case of the discrete level scheme and the NLD model. The positions of the isomers of interest are also plotted as well as the position of the last discrete level used in the calculations. The position of the latter is chosen to be higher than the $T_{1/2} = 11.1$ ns isomer excitation energy and lower than the start of the discrepancies between the level scheme and the NLD.

4. Photon strength function

In the case of $E1$ transitions, different formulations of the photon strength function (PSF) are routinely used. In our calculations, we use the generalized Lorentzian (GLO) shape as defined by Kopecky *et al.* [34]:

$$f_{\mathrm{GLO}}^{E1}(E_\gamma) = \frac{1}{3(\pi \hbar c)^2}\left[\frac{E_\gamma \widetilde{\Gamma}_{E1}(E_\gamma)}{\left(E_\gamma^2 - E_{E1}^2\right)^2 + E_\gamma^2 \widetilde{\Gamma}_{E1}^2(E_\gamma)}\right.$$
$$\left. + 0.7\frac{\widetilde{\Gamma}_{E1}(E_\gamma = 0)}{E_{E1}^3}\right]\sigma_{E1}\Gamma_{E1}, \quad (10)$$

where σ_{E1}, E_{E1}, and Γ_{E1} are respectively the strength, energy, and width of the giant electric dipole resonance (GEDR). This GEDR can be split in two components in the case of deformed nuclei. The energy and temperature dependent width $\widetilde{\Gamma}_G(E_\gamma)$ was derived by Kadmenskij *et al.* [35]:

$$\widetilde{\Gamma}_G(E_\gamma) = \frac{\Gamma_G}{E_G^2}\left(E_\gamma^2 + 4\pi^2 T^2\right), \quad (11)$$

where the nuclear temperature T is given by

$$T = \sqrt{\frac{E_n + S_n - \Delta - E_\gamma}{a(S_n)}} \quad (12)$$

and where E_n is the incident neutron energy.

For transitions other than $E1$, the standard Lorentzian (SLO) shape is used in agreement with the Brink hypothesis [36]:

$$f_{\mathrm{SLO}}^{XL}(E_\gamma) = \frac{1}{(2L+1)(\pi \hbar c)^2}\frac{\sigma_{XL}E_\gamma^{3-2L}\Gamma_{XL}^2}{\left(E_\gamma^2 - E_{XL}^2\right)^2 + E_\gamma^2 \Gamma_{XL}^2}. \quad (13)$$

The resonance parameters used in our calculations are obtained using systematic formulas compiled in Ref. [32] and are given in Table II.

B. Comparison with experimental spectra

The validation of our GEANT4/EVITA simulations is performed by comparing experimental and simulated spectra. The experimental spectra are obtained by applying a narrow energy

TABLE II. Resonance parameters used in the PSF calculations.

Transition XL	E_{XL} (MeV)	Γ_{XL} (MeV)	σ_{XL} (mb)
$E1$	14.251	4.157	468.825
$M1$	7.302	4.0	1.487
$E2$	11.221	3.986	0.354
$M2$	7.302	4.0	0.001

selection around the S_n value, $E_\Sigma \in [6.8, 7.3]$ MeV, in order to increase the signal-to-background ratio. We also apply a selection in the neutron incident energy, $E_n \in [0.08, 0.3]$ eV, which corresponds to a selection on a wide neutron resonance ($E_n = 0.1413$ eV, $J^\pi = 13/2^-$) [37]. Therefore the segmented mode is used to obtain enough statistics, but it cannot be used to determine isomeric ratios as explained in Sec. III.
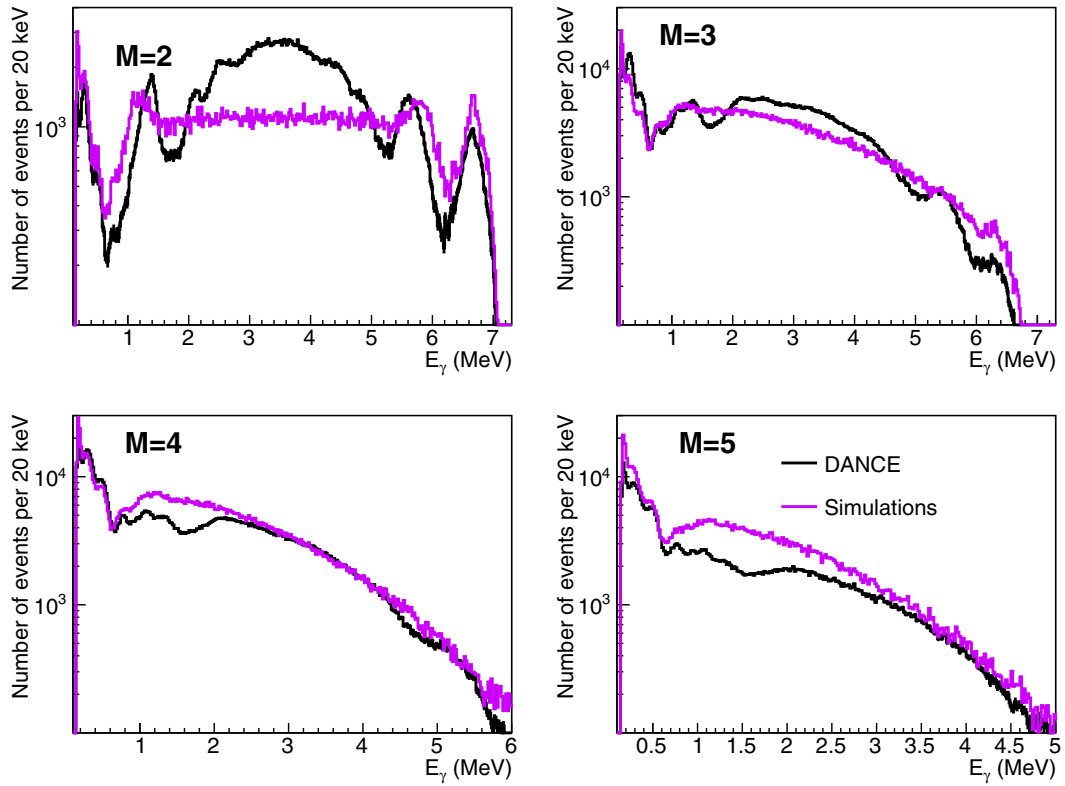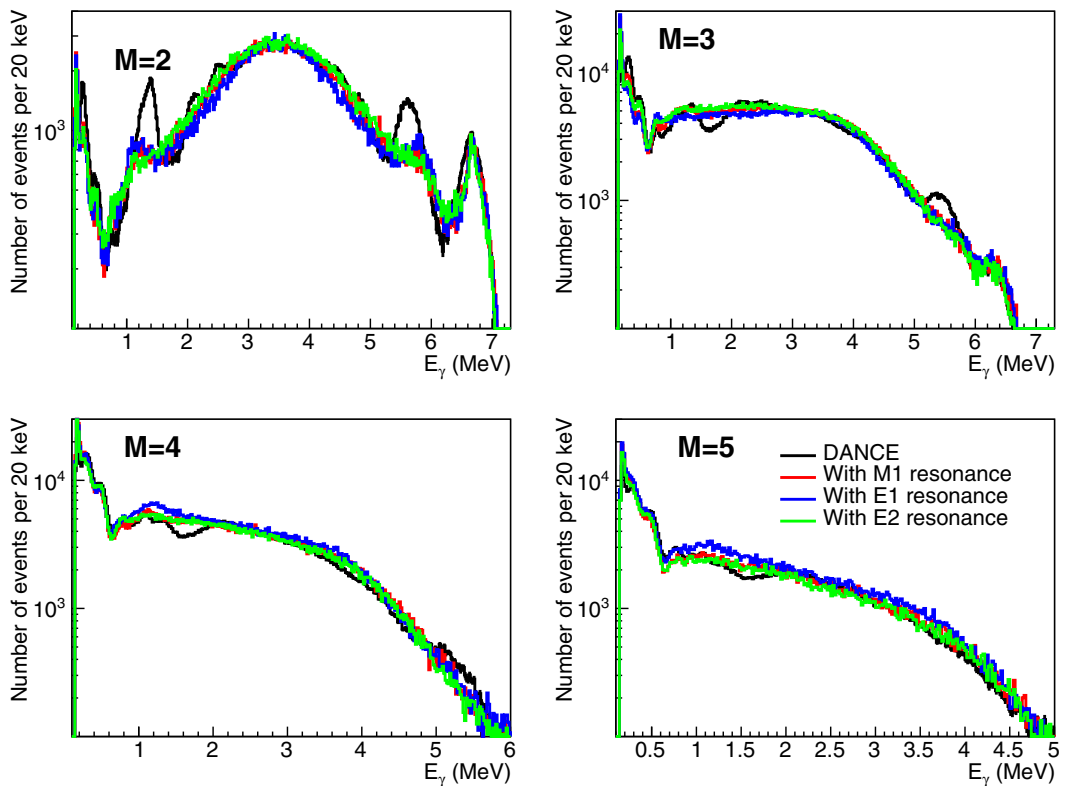
The comparisons between experimental and theoretical γ-ray spectra for multiplicities ranging from $M = 2$ to $M = 5$ are presented in Fig. 6. The simulated spectra are normalized to the same total number of detected cascades ($M \geqslant 1$). Large discrepancies are observable for $M = 2$ between the theoretical and experimental spectra. The most significant discrepancy is observed between 2 and 5 MeV in the simulated spectra. The same discrepancies have been observed in ^{177}Lu by Bečvář *et al.* [38] in a two-step cascade experiment. To obtain a better agreement between their experimental and calculated spectra using DICEBOX [39], they added a resonance in the $M1$ PSF. This resonance is unambiguously attributed to a scissor mode (SM) by the authors. The parameters of this one are $E_{SM} = 4.0$ MeV, $\Gamma_{SM} = 1.0$ MeV, and $\sigma_{SM} = 2$ mb, which corresponds to $\sum B(M1)\uparrow = 24.5\mu_N^2$. As indicated by the authors, the values of the energy and the total reduced $M1$ strength are extremely high in comparison to other published data. Indeed, according to the systematic [40] and the ^{177}Lu deformation parameters [41], the scissor resonance is expected to be located around 3.1 MeV. Similar resonances have also been observed in neutron capture experiments performed on Gd [42–45] and Dy [46,47] isotopes and on ^{238}U [22,48].

In the similar manner, we have introduced an $M1$ resonance in the PSF in order to reproduce our experimental spectra. The best agreement is obtained with the following parameters: $E_{SM} = 4.25$ MeV, $\Gamma_{SM} = 2.0$ MeV, and $\sigma_{SM} = 3.75$ mb. These values are of the same order of magnitude as the ones of Bečvář *et al.* [38]. The comparison between the experimental spectra and the spectra with an added $M1$ strength is presented in Fig. 7. The agreement is clearly better, particularly for the $M = 2$ multiplicity. Other simulations with an $M1$ resonance located at lower energies near the systematic one were performed. The experimental spectra cannot be reproduced satisfactorily with these calculations. The peaks located around 5.5 and 1.5 MeV which are clearly visible in the $M = 2$ and $M = 3$ spectra are not reproduced with our Hauser-Feshbach calculations. These peaks come mainly from the decay of the capture states down to the three quasiparticle states built from the neutron pair breaking coupled to the one quasiparticle proton state. If these levels are not included in the calculations the peaks at 1.5 and 5.5 MeV are smoothed out. A possible way to reproduce these peaks, without missing an important number of levels (see Fig. 5), is to introduce the considered experimental levels in the phenomenological NLD, but this feature is not yet implemented in our EVITA code. It is noticeable that the peaks at 0.3 and 6.8 MeV are well reproduced because the levels around 0.3 MeV are included in our calculations.

Bečvář *et al.* indicate that the resonance added to reproduce their data is unambiguously of $M1$ electromagnetic nature. With our data, we cannot make a conclusion about the nature of this resonance. Indeed, if we add an $E1$ or $E2$ resonance in the PSF with the same parameters as used for the $M1$ one,

FIG. 6. Comparison between experimental and calculated γ-ray spectra.

FIG. 7. Comparison between experimental and calculated γ-ray spectra with $M1$, $E1$, and $E2$ resonances. All the resonances have the same parameters.
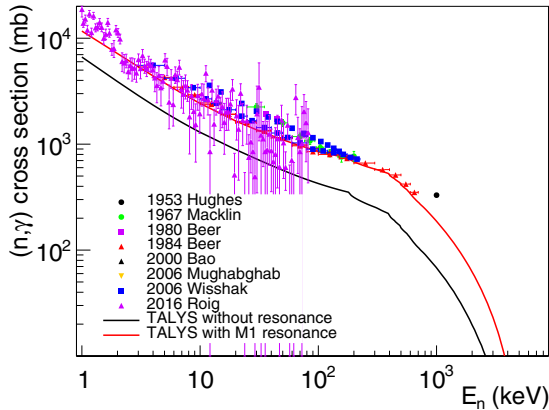
FIG. 8. Experimental data from the EXFOR database and TALYS calculations of the ^{176}Lu(n,γ) cross section with and without the added $M1$ resonance in the PSF. The PSF in the TALYS calculation are not renormalized: $G_{\mathrm{norm}} = 1$.

we obtain almost the same agreement between experimental and calculated spectra as shown in Fig. 7. Due to the very low energy resolution of the BaF$_2$ detectors and the use of the segmented mode, we cannot identify the final level of the γ cascades as Bečvář *et al.* did in their two-step cascade experiment with Ge detectors.

C. Effect of this resonance on the (n,γ) cross section

In order to reproduce the (n,γ) cross section, the PSF is generally renormalized by taking into account the experimental average radiative capture width Γ_γ and the average resonance spacing D_0. To reproduce the data on ^{176}Lu with our TALYS calculations without any additional resonance, it is necessary to renormalize the PSF by a factor of $G_{\mathrm{norm}} = 3.6$. When the resonance is added in the PSF, it is no longer necessary to renormalize this PSF to reproduce the data as shown in Fig. 8. This conclusion was previously stressed by Ullmann *et al.* [48].

In the TALYS calculations with the added $M1$ resonance in the PSF, the obtained average radiative capture width is $\Gamma_\gamma = 60$ meV. This value is compatible with our recent measurement [49], $\Gamma_\gamma = 65.8 \pm 0.2$ meV, and with Mughabghab's $\Gamma_\gamma = 63 \pm 14$ meV [37].

D. Detection efficiencies

As presented above, the detection efficiencies are determined with GEANT4/EVITA simulations of the DANCE array. The EVITA cascade is adjusted in order to reproduce the experimental data. The efficiencies ϵ_{casc} and ϵ_{iso} take into account not only the DANCE detection efficiencies (geometric and intrinsic) on a γ ray or a γ cascade but also the multiplicity cut. Indeed they correct the data for the events with multiplicities $M < 3$ and $M > 6$ which are not experimentally determined.

The cascade detection efficiency ϵ_{casc} is defined as the ratio of the number of detected cascades for $M \in [\![3,6]\!]$ in the simulated DANCE array, which is calculated by integrating the total energy spectrum in the energy range 3.5–7.5 MeV,

TABLE III. Experimental isomeric ratios.

Isomer	Expt. R_{iso} (%)
$E_{\mathrm{iso}} = 761.7$ keV $T_{1/2} = 32.8$ ns	10.5 ± 0.6
$E_{\mathrm{iso}} = 1356.9$ keV $T_{1/2} = 11.1$ ns	4.8 ± 0.6

and the total number of initial cascades calculated with EVITA. Our cascade simulations are performed with an $M1$, $E1$, or $E2$ resonance added in the corresponding PSF to reproduce the γ ray spectra as described above. As the electromagnetic nature of the resonance needed to reproduce our data is not determined, ϵ_{casc} is calculated as a mean and standard deviation over the results obtained with the different resonances. We obtain: $\epsilon_{\mathrm{casc}} = 54.9 \pm 1.1\%$.

The isomer detection efficiency ϵ_{iso} is also calculated with GEANT4 simulations using EVITA. It is defined as the ratio of the full energy peak integral of the γ rays used to evaluate $N_{\mathrm{iso}}^{\mathrm{exp}}$ summed over the multiplicities $M \in [\![3,6]\!]$ and the total number of the same γ rays in the initial cascades calculated with EVITA. In the same way as for ϵ_{casc}, ϵ_{iso} is a mean over the results of the simulations obtained with the different types of added resonances. We obtain $31.7 \pm 0.5\%$ and $38.0 \pm 0.6\%$ for the 761.7 and 1356.9 keV isomers respectively.

Other ^{177}Lu cascades obtained with the different parameters or code were tested. Even if the obtained detection efficiencies are slightly different, the deduced isomeric ratios are compatible. The uncertainty on the detection efficiencies is thus not the major one for the isomeric ratio determination.

V. RESULTS AND DISCUSSIONS

The experimental data presented in Sec. III and the detection efficiencies calculated in Sec. IV allow us to obtain the isomeric ratios summarized in Table III, following Eq. (2).

These experimental values can be compared with TALYS calculations with the parameters presented in Sec. IV and with the $M1$, $E1$, or $E2$ resonance added in the PSF. The calculated isomeric ratios are presented in Table IV for the different electromagnetic types of the added resonances and for the case without added resonance.

TABLE IV. Isomeric ratios calculated with TALYS compared to the experimental ones.

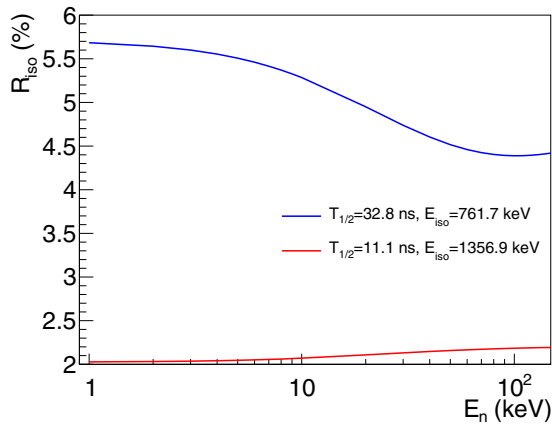| Isomer	Added resonance	Calc. R_{iso} (%)	Expt. R_{iso} (%)
$E_{\mathrm{iso}} = 761.7$ keV $T_{1/2} = 32.8$ ns	$\emptyset$	4.1	10.5 ± 0.6
	$M1$	5.7	
	$E1$	5.0	
	$E2$	6.3	
$E_{\mathrm{iso}} = 1356.9$ keV $T_{1/2} = 11.1$ ns	$\emptyset$	2.6	4.8 ± 0.6
	$M1$	2.0	
	$E1$	2.0	
	$E2$	1.6	

FIG. 9. Evolution of the isomeric ratios as a function of the incident neutron energy. Calculations performed with the $M1$ resonance added in the PSF.

Large discrepancies between experimental and evaluated isomeric ratios can be observed regardless of the addition and the nature of the added resonance. The agreement between experimental and calculated isomeric ratios is improved by adding an $E2$ resonance for the 761.7 keV isomer. On the other hand, it is better without any resonance in the case of the 1356.9 keV isomer. Calculations with different models and parameters were performed to test their impacts on the isomeric ratios.

A. Isomeric ratio calculations with TALYS

1. Evolution with neutron energy

The isomeric ratios presented in Table IV are calculated for an incident neutron energy of 1 keV, which is the minimum energy available in TALYS. In Fig. 9 the evolution of the isomeric ratios as a function of the incident neutron energy is plotted. The isomeric ratios vary slowly for neutron energies higher than 1 keV. Moreover, the lower the neutron energy, the higher the (n,γ) cross section and the neutron flux. The most important part of the statistics is thus obtained at low neutron energy. Thus it is a valid approximation to calculate the isomeric ratio at only $E_n = 1$ keV.

2. Nuclear level density model

The other NLD models available in TALYS were tested with the different XL types of the resonance added in the PSF. The default parameters of these NLD are used in our calculations [32]. These models are phenomenological (Gilbert and Cameron, back-shifted Fermi gas, generalized superfluid) and microscopic (calculations from Hartree-Fock-Bogolyubov (HFB) framework with the Skyrme interaction [50]). The results of these calculations are presented in Table V for the $E_{iso} = 761.7$ keV, $T_{1/2} = 32.8$ ns isomer and in Table VI for the $E_{iso} = 1356.9$ keV, $T_{1/2} = 11.1$ ns isomer.

As presented in Tables V and VI, the choice of the NLD has a strong impact on isomeric ratios. Indeed, the isomeric ratio ranges are [3.5,6.4] and [1.0,2.5] for the 761.7 and 1356.9 keV isomers respectively. The maximum isomeric

TABLE V. Isomeric ratios calculated with TALYS as a function of the NLD models for the $E_{iso} = 761.7$ keV, $T_{1/2} = 32.8$ ns isomer compared to the experimental value.

NLD model	Added resonance	Calc. R_{iso} (%)	Expt. R_{iso} (%)
	$\emptyset$	4.1	
Gilbert	$M1$	5.7	
and Cameron	$E1$	5.0	
	$E2$	6.3	
	$\emptyset$	4.9	
Back-shifted	$M1$	4.6	
Fermi gas	$E1$	4.3	
	$E2$	5.0	
	$\emptyset$	4.5	
Generalized	$M1$	4.9	
superfluid	$E1$	4.1	10.5 ± 0.6
	$E2$	5.5	
	$\emptyset$	3.5	
HFB from	$M1$	5.0	
Goriely's tables	$E1$	3.9	
	$E2$	5.8	
	$\emptyset$	3.9	
HFB from	$M1$	5.3	
Hilaire's tables	$E1$	4.4	
	$E2$	5.9	

ratios are obtained with the Gilbert and Cameron model but they are still strongly underestimated in comparison with the experimental ones.

TABLE VI. Isomeric ratios calculated with TALYS as a function of the NLD models for the $E_{iso} = 1356.9$ keV, $T_{1/2} = 11.1$ ns isomer compared to the experimental value.

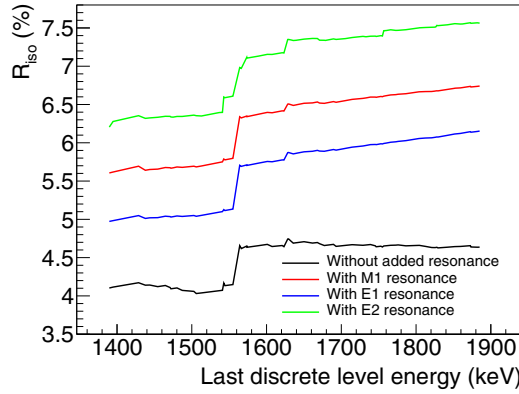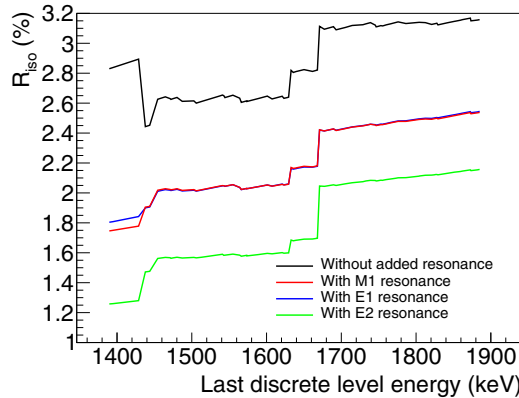| NLD model	Added resonance	Calc. R_{iso} (%)	Expt. R_{iso} (%)
	$\emptyset$	2.6	
Gilbert	$M1$	2.0	
and Cameron	$E1$	2.0	
	$E2$	1.6	
	$\emptyset$	2.3	
Back-shifted	$M1$	1.9	
Fermi gas	$E1$	1.9	
	$E2$	1.4	
	$\emptyset$	2.4	
Generalized	$M1$	1.7	
superfluid	$E1$	1.7	4.8 ± 0.6
	$E2$	1.3	
	$\emptyset$	1.8	
HFB from	$M1$	1.3	
Goriely's tables	$E1$	1.4	
	$E2$	1.0	
	$\emptyset$	2.4	
HFB from	$M1$	1.7	
Hilaire's tables	$E1$	1.7	
	$E2$	1.3	

(a) $E_{iso} = 761.7$ keV, $T_{1/2} = 32.8$ ns isomer

(b) $E_{iso} = 1356.9$ keV, $T_{1/2} = 11.1$ ns isomer

FIG. 10. Isomeric ratio evolutions as a function of the last discrete level energy.

3. *Evolution with the energy of the last discrete level*

The choice of the last discrete level taken into account in the calculations is crucial. This level is the link between the level scheme and the level density model. Indeed, the γ-ray intensity of transitions which have an initial level with an excitation energy higher than the last discrete level is determined statistically. If there are particular high-energy transitions which directly populate the isomers, they cannot be reproduced with statistical calculations. In Fig. 10, the evolution of the isomeric ratios as a function of the last discrete level energy is plotted for the case of the Gilbert and Cameron NLD model.

According to Fig. 10(a), the evolution of the isomeric ratio of the 761.7 keV isomer is flat up to 1550 keV for the different added resonance. Then a brief increase is visible around 1550 keV. It corresponds to the decay of the $J^\pi = 7/2^-$ level located at 1573.52 keV to the 761.7 keV isomer. For energies higher than 1550 keV, the isomeric ratio slowly increases.

The evolution of the isomeric ratio of the 1356.9 keV isomer as a function of the last discrete level energy [Fig. 10(b)] is flat for energies higher than 1450 keV and strongly increases around 1630 keV. It corresponds to the decay of the $J^\pi = 15/2^+$ level located at 1632.84 keV to the 1356.9 keV isomer. Then the isomeric ratio slowly increases.

TABLE VII. Isomeric ratios calculated with the CoH$_3$ code compared to the experimental ones.

Isomer	Calc. R_{iso} (%)	Expt. R_{iso} (%)
$E_{iso} = 761.7$ keV $T_{1/2} = 32.8$ ns	3.4	10.5 ± 0.6
$E_{iso} = 1356.9$ keV $T_{1/2} = 11.1$ ns	1.5	4.8 ± 0.6

The impact of the last discrete level choice is different for the two isomers. A better agreement between experimental data and calculations is obtained with an $E2$ resonance for the 761.7 keV isomer while it is worse for the 1356.9 keV isomer.

As expected, the isomeric ratios are thus very sensitive to the level scheme. The observed discrepancies between experimental and calculated isomeric ratios could indicate that the level scheme is not accurately known and transitions which populate the isomers of interest could be missing in the tabulated data.

B. Isomeric ratio calculations with CoH$_3$

Isomeric ratio calculations have also been performed with the Monte Carlo CoH$_3$ code [22]. The main difference between CoH$_3$ and EVITA/TALYS is the level density description. Indeed, in CoH$_3$ it is possible to include experimental levels in the continuous level density whereas in EVITA/TALYS the transition between discrete and continuous level density is abrupt. The CoH$_3$ calculations also include an $M1$ resonance in the PSF in order to reproduce our DANCE data in the same way as in Sec. IV. These isomeric ratios are summarized in Table VII for the two studied isomers. The calculated isomeric ratios are of the same order of magnitude as the EVITA/TALYS ratios and are not in agreement with the experimental results.

VI. CONCLUSION AND PERSPECTIVES

For the first time, isomeric ratios of the radiative capture reaction ^{176}Lu(n,γ) for two isomeric states of the ^{177}Lu compound nucleus, at 761.7 keV ($J^\pi = 5/2^-$, $T_{1/2} = 32.8$ ns) and 1356.9 keV ($J^\pi = 15/2^+$, $T_{1/2} = 11.1$ ns) have been obtained from a TOF experiment at DANCE integrated over the neutron energy range 8.5 eV–100 keV. The obtained experimental values are 10.5 ± 0.6% and 4.8 ± 0.6% for the 761.7 keV and the 1356.9 keV isomer respectively.

The detection efficiency correction was performed with GEANT4 simulations. The γ cascades used as inputs of these simulations were obtained with our EVITA code based on TALYS. The introduction of a low energy resonance in the PSF is required to reproduce the γ-ray spectra. The parameters of this resonance are $E = 4.25$ MeV, $\Gamma = 2.0$ MeV, and $\sigma = 3.75$ mb. No conclusion on the electromagnetic nature of this resonance could be deduced from our data. Thanks to the introduction of this resonance, one no longer needs to renormalize the PSF in order to reproduce the experimental ^{176}Lu(n,γ) cross section. Indeed, the calculated average radia-

tive capture width is now in agreement with the experimental one.

The experimental isomeric ratios were compared with TALYS calculations. Large discrepancies were observed between the data and the calculations. Different parameters and

models were tested without success in order to reproduce the experimental results. The level scheme, which is a key ingredient of this kind calculation, needs to be improved in order to better reproduce the data.

[1] J. Audouze, W. A. Fowler, and D. N. Schramm, Nat. Phys. Sci. **238**, 8 (1972).

[2] H. Beer, F. Käppeler, K. Wisshak, and R. Ward, Astrophys. J. Suppl. Ser. **46**, 295 (1981).

[3] N. Klay, F. Käppeler, H. Beer, and G. Schatz, Phys. Rev. C **44**, 2839 (1991).

[4] T. Kawano, P. Talou, J. E. Lynn, M. B. Chadwick, and D. G. Madland, Phys. Rev. C **80**, 024611 (2009).

[5] F. Käppeler, A. Mengoni, and R. Gallino, Nucl. Phys. A **718**, 173 (2003).

[6] K. Takahashi and K. Yokoi, At. Data Nucl. Data Tables **36**, 375 (1987).

[7] E. Segrè and A. C. Helmholz, Rev. Mod. Phys. **21**, 271 (1949).

[8] J. R. Huizenga and R. Vandenbosch, Phys. Rev. **120**, 1305 (1960).

[9] M. Jandel, B. Baramsai, T. A. Bredeweg, A. Couture, A. Hayes, T. Kawano, S. Mosby, G. Rusev, I. Stetcu, T. N. Taddeucci *et al.*, EPJ Web Conf. **93**, 02019 (2015).

[10] I. Stetcu, P. Talou, T. Kawano, and M. Jandel, Phys. Rev. C **88**, 044603 (2013).

[11] X. Ledoux, J. Sigaud, T. Granier, J.-P. Lochard, Y. Patin, P. Pras, C. Varignon, J.-M. Laborie, Y. Boulin, and F. Gunsing, Eur. Phys. J. A **27**, 59 (2006).

[12] J. Rekstad, T. S. Tveter, and M. Guttormsen, Phys. Rev. Lett. **65**, 2122 (1990).

[13] R. K. Sheline, L. Bergholt, M. Guttormsen, J. Rekstad, and T. S. Tveter, Phys. Rev. C **51**, 3078 (1995).

[14] L. Aldea, F. Bečvàr *et al.*, Czec. J. Phys. B **28**, 17 (1978).

[15] C. Bishop, H. V onach, and J. Huizenga, Nucl. Phys. **60**, 241 (1964).

[16] C. Heiser and K. Alexander, Nucl. Phys. **70**, 415 (1965).

[17] K. Wisshak, F. Voss, F. Käppeler, L. Kazakov, F. Bečvàr, M. Krtička, R. Gallino, and M. Pignatari, Phys. Rev. C **73**, 045807 (2006).

[18] K. Wisshak, F. Voss, C. Arlandini, F. Käppeler, and L. Kazakov, Phys. Rev. C **61**, 065801 (2000).

[19] M. Jandel, T. Bredeweg, E. Bond, M. Chadwick, A. Couture, J. O'Donnell, M. Fowler *et al.*, Los Alamos National Laboratory Report No. LA-UR-13-20355 2013 (unpublished), http://permalink.lanl.gov/object/tr?what=info:lanl-repo/lareport/LA-UR-13-20355.

[20] M. Jandel, T. Bredeweg, E. Bond, M. Chadwick, A. Couture, J. O'Donnell, M. Fowler *et al.*, in *Proceedings of the Fifth International Conference on Fission and Properties of Neutron-Rich Nuclei* (World Scientific, Singapore, 2013), pp. 416–423.

[21] A. Koning, S. Hilaire, and M. Duijvestijn, in *Proceedings of the International Conference on Nuclear Data for Science and Technology*, edited by O. Bersillon, F. Gunsing, E. Bauge, R. Jacqmin, and S. Lera (EDP Sciences, Les Ulis, France, 2008), pp. 211–214.

[22] T. Kawano, P. Talou, M. B. Chadwick, and T. Watanabe, J. Nucl. Sci. Technol. **47**, 462 (2010).

[23] A. Michaudon and S. Wender, Los Alamos National Laboratory Report No. LA-UR-90-4355, 1990 (unpublished), http://lib-www.lanl.gov/cgi-bin/getfile?00328726.pdf

[24] M. Heil, R. Reifarth, M. Fowler, R. Haight, F. Käppeler, R. Rundberg, E. Seabury, J. Ullmann, J. Wilhelmy, and K. Wisshak, Nucl. Instrum. Methods Phys. Res., Sect. A **459**, 229 (2001).

[25] J. M. Wouters, A. Vicente, T. Bredeweg, E. Esch, R. Haight, R. Hatarik, J. O'Donnell, R. Reifarth, R. Rundberg *et al.*, IEEE Trans. Nucl. Sci. **53**, 880 (2006).

[26] F. Kondev, Nucl. Data Sheets **98**, 801 (2003).

[27] P. Petkov, W. Andrejtscheff, H. Börner, S. Robinson, N. Klay, and S. Yamada, Nucl. Phys. A **599**, 505 (1996).

[28] T. Kibédi, T. Burrows, M. Trzhaskovskaya, P. Davidson, and C. Nestor, Jr., Nucl. Instrum. Methods Phys. Res., Sect. A **589**, 202 (2008).

[29] S. Agostinelli, J. Allison, K. Amako, J. Apostolakis, H. Araujo, P. Arce, M. Asai, D. Axen, S. Banerjee, G. Barrand *et al.*, Nucl. Instrum. Methods Phys. Res., Sect. A **506**, 250 (2003).

[30] M. Jandel, T. Bredeweg, A. Couture, M. Fowler, E. Bond, M. Chadwick, R. Clement, E.-I. Esch, J. O'Donnell, and R. Reifarth, Nucl. Instrum. Methods B **261**, 1117 (2007).

[31] G. Boutoux, B. Jurado, V. Méot, O. Roig, L. Mathieu, M. Aïche, G. Barreau, N. Capellan, I. Companis, S. Czajkowski *et al.*, Phys. Lett. B **712**, 319 (2012).

[32] R. Capote, M. Herman, P. Oblozinski, P. Young, S. Goriely, T. Belgya, A. Ignatyuk, A. Koning, S. Hilaire, V. Plujko *et al.*, Nucl. Data Sheets **110**, 3107 (2009).

[33] A. Gilbert and A. G. W. Cameron, Can. J. Phys. **43**, 1446 (1965).

[34] J. Kopecky, M. Uhl, and R. E. Chrien, Phys. Rev. C **47**, 312 (1993).

[35] S. G. Kadmenskij, V. P. Markushev, and V. I. Furman, Sov. J. Nucl. Phys. **37**, 165 (1983).

[36] D. M. Brink, Ph.D. thesis, Oxford University, 1955 (unpublished).

[37] S. F. Mughabghab, *Atlas of Neutron Resonances* (Elsevier Science, Amsterdam, 2007).

[38] F. Bečvář, M. Krtička, I. Tomandl, and S. Valenta, EPJ Web Conf. **93**, 01054 (2015).

[39] F. Bečvář, Nucl. Instrum. Methods Phys. Res., Sect. A **417**, 434 (1998).

[40] K. Heyde, P. von Neumann-Cosel, and A. Richter, Rev. Mod. Phys. **82**, 2365 (2010).

[41] P. Moller, J. Nix, W. Myers, and W. Swiatecki, At. Data Nucl. Data Tables **59**, 185 (1995).

[42] A. Chyzh, B. Baramsai, J. A. Becker, F. Bečvář, T. A. Bredeweg, A. Couture, D. Dashdorj, R. C. Haight, M. Jandel, J. Kroll *et al.*, Phys. Rev. C **84**, 014306 (2011).

[43] B. Baramsai, J. Kroll, G. E. Mitchell, U. Agvaanluvsan, F. Bečvář, T. A. Bredeweg, A. Chyzh, A. Couture, D. Dashdorj, R. C. Haight *et al.*, Phys. Rev. C **87**, 044609 (2013).

[44] J. Kroll, B. Baramsai, G. E. Mitchell, U. Agvaanluvsan, F. Bečvář, T. A. Bredeweg, A. Chyzh, A. Couture, D. Dashdorj, R. C. Haight *et al.*, Phys. Rev. C **88**, 034317 (2013).

[45] J. Kroll, S. Valenta, M. Krtička, F. Bečvář, I. Tomandl, and G. E. Mitchell, EPJ Web Conf. **93**, 01036 (2015).

[46] M. Krtička, F. Bečvář, J. Honzátko, I. Tomandl, M. Heil, F. Käppeler, R. Reifarth, F. Voss, and K. Wisshak, Phys. Rev. Lett. **92**, 172501 (2004).

[47] B. Baramsai, F. Bečvář, T. Bredeweg, R. Haight, M. Jandel, J. Kroll, M. Krtička, G. Mitchell, J. O'Donnell, R. Rundberg *et al.*, EPJ Web Conf. **93**, 01037 (2015).

[48] J. L. Ullmann, T. Kawano, T. A. Bredeweg, A. Couture, R. C. Haight, M. Jandel, J. M. O'Donnell, R. S. Rundberg, D. J. Vieira, J. B. Wilhelmy *et al.*, Phys. Rev. C **89**, 034603 (2014).

[49] O. Roig, M. Jandel, V. Méot, E. M. Bond, T. A. Bredeweg, A. J. Couture, R. C. Haight, A. L. Keksis, R. S. Rundberg, J. L. Ullmann *et al.*, Phys. Rev. C **93**, 034602 (2016).

[50] S. Goriely, S. Hilaire, and A. J. Koning, Phys. Rev. C **78**, 064307 (2008).